The Planetary Boundary Layer above a Change in Surface Roughness

P. A. TAYLOR

Dept. of Mathematics, University of Toronto, Canada

(Manuscript received 19 August 1968, in revised form 22 December 1968)

ABSTRACT

A mixing length model is used to relate the turbulent shear stress to the mean velocity field within the planetary boundary layer above a change in surface roughness under conditions of neutral thermal stability. This model gives rise to a parabolic system of partial differential equations. Numerical solutions are given for the case of flow above a step change in surface roughness across a line perpendicular to the geostrophic wind direction. These results show that a very long fetch is required for a true equilibrium flow to exist above the new, downwind surface. In particular, the surface wind direction adjusts only slowly to the new conditions. This suggests that experimental observations of the angle between the surface and geostrophic wind directions in supposedly nondeveloping flows may well have been affected by surface roughness changes well upstream of the experimental site. Some comparisons are made with numerical results for internal boundary layers within the shallower surface layer of the atmosphere.

1. Introduction

The problem of flow above a change in surface roughness has been considered in the case of flow close to the ground by Elliott (1958), Panofsky and Townsend (1964) and Taylor (1967), using assumed forms for the velocity or shear stress profiles within an internal boundary layer developing downstream of the roughness change. Nickerson (1968) and Taylor (1969a) have considered the same problem numerically, Nickerson considering a step change in surface shear stress and Taylor a step change in the surface roughness length. All these papers have dealt with the case where the upstream flow is a constant shear stress layer under conditions of neutral thermal stability with a logarithmic velocity profile. Blackadar *et al.*[1] and Miyake (1961) have considered the effects of non-neutral thermal stability.

The aim of the present work is to investigate the effects of changes in surface roughness on a deeper layer and so be able to predict flow development further downstream. Nickerson (1968) gives a very approximate analytic treatment of this case. As in most of the earlier work neutral thermal stability is assumed and a mixing length approach is adopted and used to relate the shear stress to the mean flow field. Unlike the case of the constant stress layer, the form of the mixing length l to be used is not well established and this problem is investigated in a companion paper (Taylor, 1969b), hereafter referred to as A. The form adopted there is

$$l(z)=\frac{k(z+z_i)}{1+kz/\lambda}, \tag{1}$$

where k is von Kármán's constant and z_i is the local value of the surface roughness length, taken to be z_0 for $x<0$ and z_i for $x>0$. The coordinate system is taken with z representing the vertical height, x the distance downstream of the roughness change in the direction of the geostrophic wind, and y horizontal and perpendicular to the x axis. Only the case of a step change in surface roughness across a line perpendicular to the geostrophic wind direction is considered here. The parameter λ, equal to the maximum value of l, was assumed in A to be a function of the roughness Rossby number $\mathrm{Ro}(=G/fz_i)$ expressed by

$$\lambda=\frac{G}{f}E(\mathrm{Ro}), \tag{2}$$

where f is the Coriolis parameter and G the geostrophic wind speed. An attempt was made in A to determine the form of the empirical function $E(\mathrm{Ro})$ but it was not entirely successful. The roughness change flow was investigated assuming that E is a constant (0.0004). If E were not constant in the equilibrium flow situation this would mean that E would vary with both x and z in the roughness change flow. It is suggested in A that λ will depend primarily on boundary layer thickness and we may anticipate that for comparatively small downstream distances, where the boundary layer thickness will not have been appreciably changed, a constant value for E will be satisfactory; far downstream, however, where we are approaching the new equilibrium flow, it will be less realistic.

[1] A. K. Blackadar, P. E. Glass and H. A. Panofsky, 1967: The effect of stability on the wind profile under conditions of inhomogeneous terrain roughness. Paper presented at U. S. Atomic Energy Commission Meteorological Information Meeting, Chalk River.

2. Equations and method of solution

Using the usual boundary layer approximations the system of equations governing the flow is parabolic and is given, for example, by Haltiner and Martin (1957, p. 219). In the present notation (see Appendix 1), non-dimensionalizing with respect to z_0 and G, and replacing the pressure gradient by the equivalent geostrophic wind term, the momentum equations are

$$U'\frac{\partial U'}{\partial x'}+W'\frac{\partial U'}{\partial z'}=\frac{V'}{\mathrm{Ro}}+\frac{\partial \tau_x'}{\partial z'}, \tag{3}$$

$$U'\frac{\partial V'}{\partial x'}+W'\frac{\partial V'}{\partial z'}=\frac{(1-U')}{\mathrm{Ro}}+\frac{\partial \tau_y'}{\partial z'}, \tag{4}$$

where primes are used to denote dimensionless variables and τ_x, τ_y are the horizontal components of the kinematic shear stress. The continuity condition, assuming constant density, has the form

$$\frac{\partial U'}{\partial x'}+\frac{\partial W'}{\partial z'}=0. \tag{5}$$

The mixing length relations, as given in A, are

$$\tau_x'=\tau'^{\frac{1}{2}}l'\frac{\partial U'}{\partial z'}, \tag{6}$$

$$\tau_y'=\tau'^{\frac{1}{2}}l'\frac{\partial V'}{\partial z'}, \tag{7}$$

where

$$\tau'^2=\tau_x'^2+\tau_y'^2. \tag{8}$$

We wish to solve these equations under the boundary conditions

$$U'=V'=W'=0 \quad \text{on} \quad z'=0, \tag{9}$$

$$U'\to 1, \quad V'\to 0 \quad \text{as} \quad z\to\infty, \tag{10}$$

and the initial conditions $U'=U_0'(z)$, $V'=V_0'(z)$ on $x'=0$, where $U_0'(z')$, $V_0'(z')$ is the equilibrium velocity profile for the upstream roughness, determined in the manner outlined in A. The wind hodograph, mixing length and eddy viscosity profiles are shown in Fig. 1 for $\mathrm{Ro}=10^7$.

The method used to obtain numerical solutions to the equations is basically to first replace the z' derivatives by finite differences to give a system of ordinary differential equations in U_I and V_I, where U_I, V_I are the x' and y' components of velocity at fixed vertical heights. This method is sometimes called the "method of lines." Close to the ground the velocity profiles will be of an essentially logarithmic form and a logarithmic spacing of the vertical finite difference points or horizontal lines would be appropriate; further out, a linear vertical scale is the natural one. In view of this difference in appropriate scales we have developed a finite difference

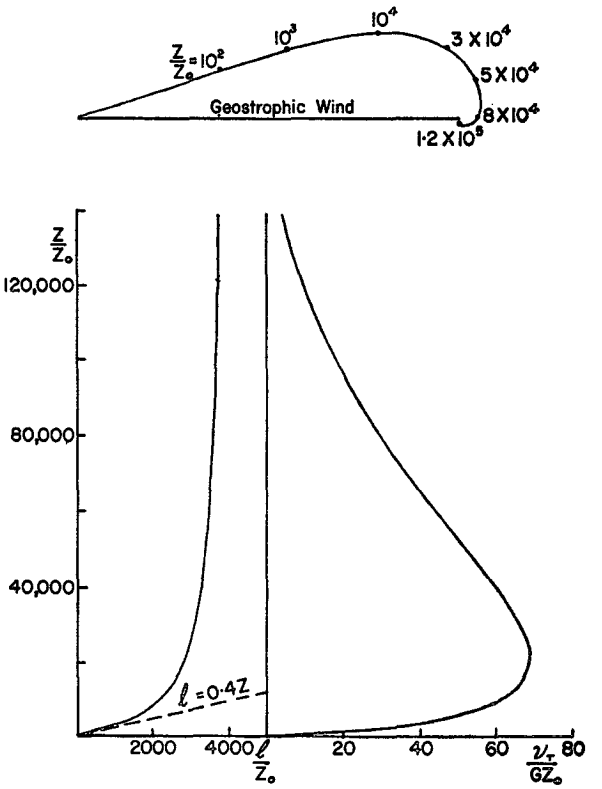

FIG. 1. Wire hodograph, mixing length and eddy viscosity profiles for upstream conditions: $\mathrm{Ro}=10^7$, $E=0.0004$.

scheme based on a logarithmic scaling from the ground up to an intermediate height, denoted by z_N and a linear scale above this. (A value of approximately 5000 was used for z_N in the results presented here.) The lower region is dealt with by a change in the vertical coordinate and a new variable ζ is introduced, defined by

$$\zeta=\ln(z'+1). \tag{11}$$

Eqs. (3)–(7) then become:

$$U'\frac{\partial U'}{\partial x'}+e^{-\zeta}W'\frac{\partial U'}{\partial \zeta}=\frac{V'}{\mathrm{Ro}}+e^{-\zeta}\frac{\partial \tau_x'}{\partial \zeta}, \tag{12}$$

$$U'\frac{\partial V'}{\partial x'}+e^{-\zeta}W'\frac{\partial V'}{\partial \zeta}=\frac{(1-U')}{\mathrm{Ro}}+e^{-\zeta}\frac{\partial \tau_y'}{\partial \zeta}, \tag{13}$$

$$\frac{\partial U'}{\partial x'}+e^{-\zeta}\frac{\partial W'}{\partial \zeta}=0, \tag{14}$$

$$\tau_x'=\tau'^{\frac{1}{2}}l'e^{-\zeta}\frac{\partial U'}{\partial \zeta}, \tag{15}$$

$$\tau_y'=\tau'^{\frac{1}{2}}l'e^{-\zeta}\frac{\partial V'}{\partial \zeta} \tag{16}$$

An additional "wall layer" is introduced close to the

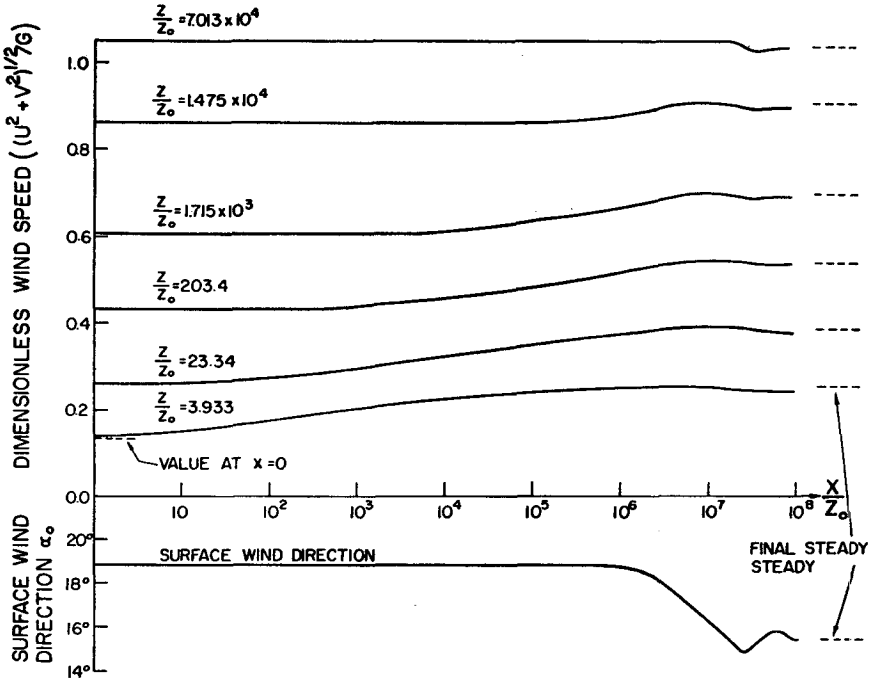

FIG. 2. Downstream variation of wind speed and surface wind direction: $m=0.1$, $\mathrm{Ro}=10^7$, $E=0.0004$.

ground in order to speed up the downstream integration of the equations. A height z_{IS}, which may be changed in steps as we integrate downstream, is chosen below which the shear stress is assumed to be constant. The value of z_{IS} used increased from small values at $x=0$ to 1715 for $x/z_0=10^7$. Details of the scheme are given in Appendix 2. A typical integration for x' varying from 0 to 4×10^7 took about 7 min on the University of Toronto's IBM 7094 computer.

3. Numerical results

Numerical results have been obtained for a range of values of $m(=z_1/z_0)$, the ratio of downstream to upstream roughness. Results for $m=0.1$ and $m=10$ are

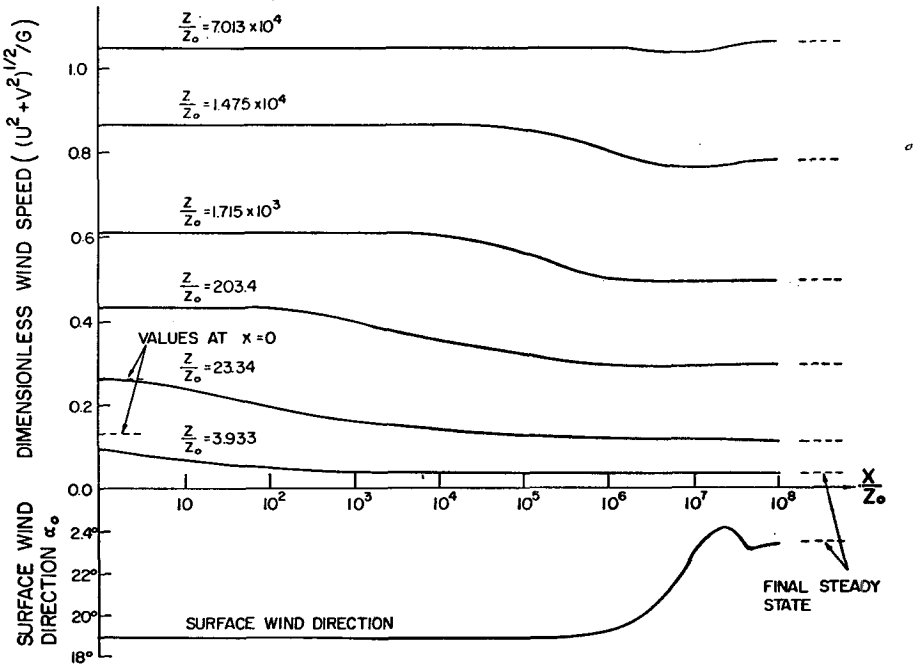

FIG. 3. Downstream variation of wind speed and surface wind direction: $m=10$, $\mathrm{Ro}=10^7$, $E=0.0004$.

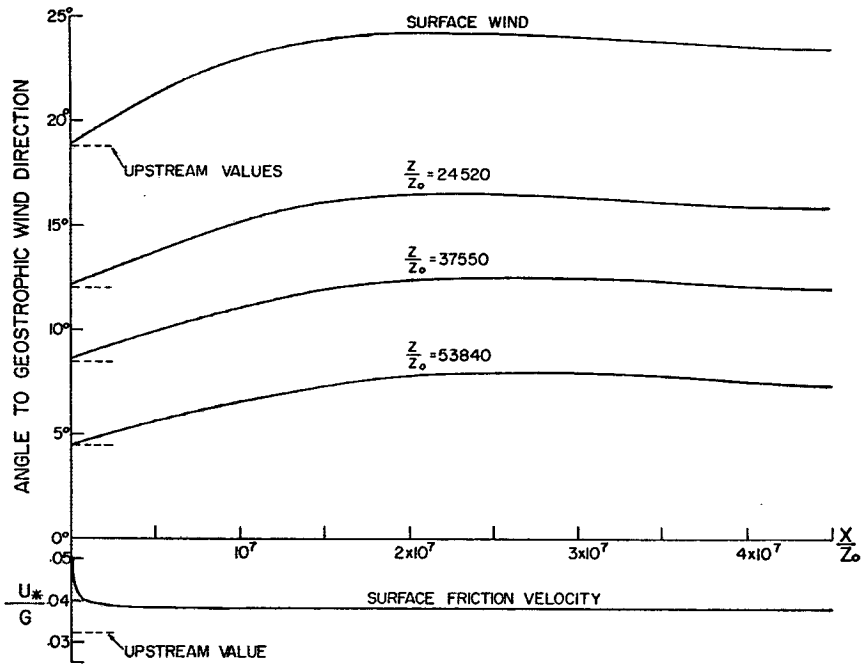

FIG. 4. Downstream variation in wind direction at various heights: $m=10$, $\mathrm{Ro}=10^7$, $E=0.0004$.

presented in Figs. 2–6, while Fig. 7 contains results obtained for comparison with the surface layer model. In all the cases presented here the upstream profiles corresponded to $\mathrm{Ro}=10^7$, $E=0.0004$.

Figs. 2 and 3 show the variations in wind speed at certain fixed heights and also the variation in surface wind direction with downstream distance. The angle between the surface and geostrophic wind direction is denoted by α_0. The wind speeds at some of the lower heights for large values of x/z_0 are interpolated values based on the assumption of a logarithmic velocity profile near the ground. The assumption of a constant stress layer in this region also gives rise to slight corrections in the values obtained for surface wind direction. The corrections were based on a downstream integration with no roughness change (i.e., $m=1$) using the same numerical integration scheme. It was found that a reduction of about 1.3° in α_0 took place corresponding to the assumption of a constant stress layer out to $z'=1700$. This did not give rise to any significant perturbation of the flow in the $m=1$ integration.

The results show that the logarithmic scaling of the x/z_0 axis used in the figures is appropriate for considerations of wind speed but that the wind direction remains essentially unchanged, in both the rough to smooth and smooth to rough cases until x/z_0 is approximately 10^6. The damped oscillations far downstream are a result of the action of Coriolis forces and in both cases the final equilibrium state is achieved by $x/z_0=10^8$. The final steady states were calculated independently in the manner described in A. The oscillatory nature of the approach to the final steady state is interesting and not entirely unexpected.

Fig. 4 shows the downstream variation in wind direction at various heights for $m=10$ and also, for comparison, the downstream variation in surface friction velocity. This time x/z_0 is scaled linearly and shows that this is the appropriate scaling for wind direction considerations. It also shows that the changes in angle occur more or less uniformly across the layer rather than spreading up from the surface as is the case with the wind speed modifications. We may see that the surface friction velocity is nearly equal to its final equilibrium value by $x/z_0=2\times10^6$ or even less, while the angles are much slower to adjust.

It may be seen from Figs. 2 and 3 that the changes in angle takes place over the range $x/z_0=10^6-10^8$ in both

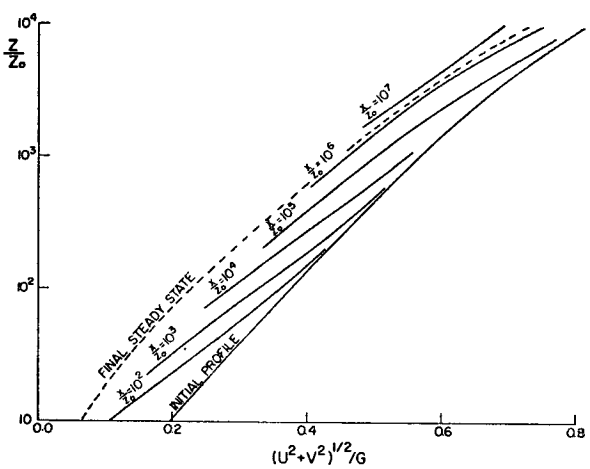

FIG. 5. Downstream variation in wind profile: $m=10$, $\mathrm{Ro}=10^7$, $E=0.0004$.

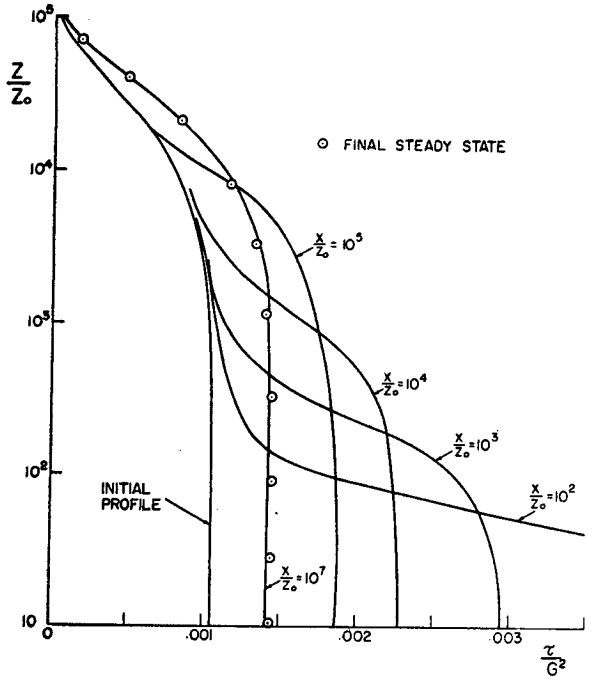

FIG. 6. Downstream variation in shear stress distribution: $m=10$, $\mathrm{Ro}=10^7$, $E=0.0004$.

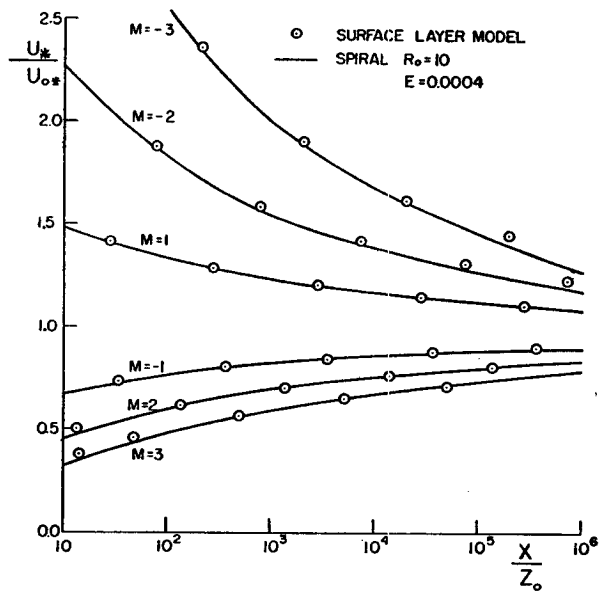

FIG. 7. Downstream variation of surface friction velocities.

cases, i.e., for rough to smooth flow, $m=0.1$, and smooth to rough flow, $m=10$. Investigations of other values of m show the changes taking place in the same range.

If we return to Eqs. (3) and (4) and consider the orders of magnitude of the Coriolis and momentum terms, which will be the important ones in this respect, we have for momentum $1/L'$, where L' is the dimensionless length scale of the downstream flow modification, and for Coriolis forces 1/Ro. If these terms are to balance we must have

$$L' \approx \mathrm{Ro}. \tag{17}$$

The results presented here are in agreement with this prediction as are some preliminary results presented by Taylor (1967) for different values of upstream Rossby number.

The wind speed results may also be presented in the form of wind profiles as is done in the case of $m=10$ in Fig. 5. This is most suitable for small heights ($z/z_0<10^4$) and moderate downstream distances ($x/x_0<10^7$) where the oscillations associated with the changes in wind direction are not important. It can be seen in Fig. 5 that the profile at $x/z_0<10^7$ lies outside the "region" bounded by the initial and final profiles. The lower limit to which the profiles have been drawn corresponds to the point below which a constant shear stress layer was assumed. The profiles in this region would be approximately logarithmic. Tests using shallower constant stress layers indicated that the errors associated with this assumption were negligible for the results presented.

Fig. 6 shows the downstream variations in shear stress profiles in the case $m=10$, again with $\mathrm{Ro}=10^7$ and $E=0.0004$. As with the other results presented the present analysis is successful in tracing the development right through to the final steady state. Some idea of the growth rate of the internal boundary layer can be obtained from this figure. The roughness change effects spread out rapidly at first and by $x/z_0=10^2$ have modified the flow out to $z/z_0=10^2$. Further downstream the growth rate slows to something like the accepted 1:10 slope. The rapid initial growth is at least partially due to approximations introduced into the model. These are the boundary layer approximation and the step change from z_0 to z_1 in the mixing length. Note that $10^2 z_0$ is only $10 z_1$ in this instance.

Fig. 7 gives a comparison of surface friction velocities obtained using the spiral model adopted here with results obtained with a surface layer model with $l=k(z+z_0)$ and an upstream logarithmic profile. We denote the upstream friction velocity by u_{0*}. [Following Panofsky and Townsend (1964), we use the notation $M=\ln(z_0/z_1)$.] The surface layer results are given by Taylor (1969a). The results are in very good agreement with each other especially as far as $x/z_0=10^5$. It should be remarked that there is a difference in the basic flow situation in that it is the surface wind that is perpendicular to the roughness change in the surface layer model but the geostrophic wind in the spiral model. This means that the surface wind is initially at 71.2° to the roughness change in the spiral case and so the distance travelled above the new roughness by a parcel of air close to the ground is not x but $x$cosecant 71.2° or approximately $1.057x$. This is hardly detectable with the logarithmic scaling used in Fig. 7.

The good agreement between results for the surface layer and spiral models prompts the question of how good the surface layer model is and how necessary is the use of the somewhat more cumbersome spiral model in any given application. If we look at the assumptions made in the surface layer model and compare them with the "Leipzig Wind Profile" (Lettau, 1950), we see that the assumption of approximately constant shear stress is valid to a considerably greater height than the assumption that

$$l=0.4(z+z_0). \tag{18}$$

If we consider the upstream profile assumed here with $\mathrm{Ro}=10^7$ and $E=0.0004$, the shear stress is approximately (within 10%) constant for $z'<4\times10^3$ (Fig. 6). At this height, however, the value of l' used in the spiral model is approximately 1140 while the surface layer value is 1600. For rougher surfaces and lower values of Ro, we may expect from A that E will take higher values and that these differences in l will be greater. This would suggest that some type of hybrid model, with the assumption of constant shear stress in the equilibrium state and an l of a form similar to Eq. (1) may well be useful in investigations of roughness change flows on an intermediate scale. The main objection to simply using the surface layer form for l would be that in any extension to include diffusion (of heat, water vapor or pollutant) within the internal boundary layer we would be using too high a diffusion coefficient at large heights.

For many natural surfaces, with z_0 ranging from 0.1 to 10 cm, it is reasonable to assume that for heights up to $\sim$50 m the shear stress is approximately constant under equilibrium flow conditions; thus, for internal boundary layer effects taking place within $\sim$ 500 m of the roughness change the surface layer model or some modification of it will probably be satisfactory. We can probably count on a height of at least 100 m over which there is no significant change in wind direction, but at heights of the order of 100 m the shear stress may no longer be approximately parallel to the velocity and the simplified two-dimensional model will become invalid. Thus, although we do not perhaps need as accurate a solution throughout the entire spiral layer as that proposed here, the effects of Coriolis forces are already important at heights of about 100 m not because the forces themselves produce any significant effect on the flow modification in this range but because they are important in forming the structure of the upstream equilibrium flow. Devious means could probably be employed to circumvent the necessity of the full spiral model but unless a large number of flow modification calculations were envisaged the full spiral model could be used almost as easily.

4. Conclusion

We have used a mixing length model to represent the flow in the planetary boundary layer above a change in surface roughness. At present, reliable measurements of shear stress and turbulent intensities within either the planetary boundary layer or within internal boundary layers are not readily available and the use of Eqs. (6) and (7) must be regarded as a tentative hypothesis. We may expect this to at least give some reasonable first approximation to the real situation and the use of more complicated relations between mean flow and turbulent quantities must await their experimental justification. We have also restricted ourselves to cases of neutral thermal stability and assumed the air to be of constant density. Subject to these restrictions and qualifications the results presented here will be useful in giving estimates of the fetch required for the establishment of equilibrium flow after a roughness change, especially with regard to the differences between the behavior of the surface wind direction and the surface friction velocity. The paper is also intended to demonstrate that basically quite straightforward numerical techniques can be used in theoretical investigations of this type of problem without excessive use of computer time. More sophisticated methods could be used to save computer time if a large number of runs were required.

Acknowledgments. An initial investigation of this problem was undertaken by the author while at the Department of Mathematics, University of Bristol, with support from the Central Electricity Generating Board as part of a Ph.D. thesis under the supervision of Dr. A. R. Paterson. Later investigations at the University of Toronto have been supported by the National Research Council of Canada.

APPENDIX 1

Notation

(Primes are used to denote nondimensional quantities where nondimensionalization is with respect to z_0 and G.)

E(Ro)	parameter in mixing length model
f	Coriolis parameter
G	geostrophic wind speed
h	parameter in mixing length form ($=\lambda/k$)
k	von Kármán's constant (0.4)
l	mixing length
L	length scale of flow modification
m	ratio of downstream to upstream roughness lengths (z_1/z_0)
M	roughness change parameter [$=\ln(z_0/z_1)$]
Ro	roughness Rossby number ($=G/fz_0$)
u_*	surface friction velocity
u_1,v_1	x and y components of surface friction velocity.
u_{0*}	upstream friction velocity
U,V	mean horizontal velocity components
U_0,V_0	upstream mean velocity profile
U_I,V_I,W_I	values of U', V', W' at discretization points
W	vertical mean velocity component

x,y	horizontal space coordinates
z	vertical space coordinate
z_i	local roughness length
z_0,z_1	upstream and downstream roughness lengths
z_I	value of z' at discretization points
z_{IS}	height to which a constant shear stress is assumed
z_N	interface between logarithmic and linear finite difference schemes
z_{NN}	upper limit of region considered
α_0	angle between surface and geostrophic wind directions
$\Delta\zeta,\Delta z$	finite difference line spacings
λ	maximum value of mixing length
ν_T	eddy viscosity
τ_x,τ_y	horizontal components of kinematic shear stress
τ	magnitude of kinematic shear stress, equal to $(\tau_x^2+\tau_y^2)^{\frac{1}{2}}$
ζ	logarithmic vertical scale $[=\ln(z'+1)]$
ζ_I	value of ζ at discretization points.

APPENDIX 2

Details of Numerical Method

The basis of the method used to solve Eqs. (12)–(16) in the lower region ($z'\leq 4973$) and Eqs. (3)–(8) in the upper region ($4973\leq z'\leq 148{,}300$) is to replace the ζ or z derivatives by finite difference approximations to give a set of ordinary differential equations in dU_I/dx and dV_I/dx where U_I and V_I are the values of U' and V' at the discretization points z_I on the z' axis. We also denote the value of W' at z_I by W_I. The resulting system of ordinary differential equations may then be solved numerically using a version of the Runge-Kutta method with the ability to adjust its step length (in the x coordinate) to give results satisfying a given error per unit step criterion. While this is an inefficient way to solve systems of parabolic partial differential equations (it takes about three times as long as a simple explicit method in this case), it is reasonably foolproof and saves considerable time, personal and computer, that would be otherwise necessary in determining step sizes compatible with numerical stability. The use of implicit schemes for the system of equations is extremely cumbersome. As a part of the solution method we require a means of calculation dU_I/dx and dV_I/dx at the discretization points from the velocity profiles at a fixed value of x.

The region close to the ground is assumed to be a constant stress layer and we have to use special equations for dU_{IS}/dx and dV_{IS}/dx. If the spacing of the ζ lines is $\Delta\zeta$, then $\zeta_{IS}=IS\cdot\Delta\zeta$. The velocity profile in $0\leq\zeta\leq\zeta_{IS}$ is given by

$$U'=\frac{u_1'}{kh'}\left[z'+(h'-m)\ln\left(\frac{z'+m}{m}\right)\right], \tag{A1}$$

$$V'=\frac{v_1'}{kh'}\left[z'+(h'-m)\ln\left(\frac{z'+m}{m}\right)\right], \tag{A2}$$

where h is a parameter in the mixing length form $(=\lambda/k)$ and u_1' and v_1', the components of the surface friction velocity, are given by

$$\tau_x'=u_1'\tau'^{\frac{1}{2}},\quad \tau_y'=v_1'\tau'^{\frac{1}{2}}. \tag{A3}$$

In Eqs. (A1) and (A2) we assume that only u_1' and v_1' are functions of x and so, using the continuity equation to obtain W_{IS} in terms of du_1'/dx and Eq. (A1) to relate dU_{IS}/dx and du_1'/dx, we obtain

$$W_{IS}=-A\frac{dU_{IS}}{dx}, \tag{A4}$$

where

$$A=\frac{0.5z_{IS}^2+(h'-m)\{(z_{IS}+m)\ln[(z_{IS}+m)/m]-z_{IS}\}}{\{z_{IS}+(h'-m)\ln[(z_{IS}+m)/m]\}}. \tag{A5}$$

This can now be substituted into the finite difference representation of Eq. (12) to obtain an expression for dU_{IS}/dx, i.e.,

$$\frac{dU_{IS}}{dx}=[(V_{IS}/\mathrm{Ro})+e^{-\zeta_{IS}}DTX_{IS}]/(U_{IS}-e^{-\zeta_{IS}}A\cdot DU_{IS}), \tag{A6}$$

where the expressions for DTX_{IS} and DU_{IS} are obtained from the finite difference formulae:

$$DU_I=(U_{I+1}-U_{I-1})/2\Delta\zeta, \tag{A7}$$

$$DV_I=(V_{I+1}-V_{I-1})/2\Delta\zeta, \tag{A8}$$

$$D2U_I=(U_{I+1}-2U_I+U_{I-1})/(\Delta\zeta)^2, \tag{A9}$$

$$D2V_I=(V_{I+1}-2V_I+V_{I-1})/(\Delta\zeta)^2, \tag{A10}$$

$$DTX_I=2l'(z_I)\left[\left(\frac{dl'}{d\zeta}\right)_{\zeta=\zeta_I}-l'(z_I)\right]e^{-2\zeta_I}(DU_I^2+DV^{I2})^{\frac{1}{2}}DU_I+l'^2(z_I)e^{-2\zeta_I}[(DU_ID2U_I+DV_ID2V_I)DU_I/(DU_I^2+DV_I^2)^{\frac{1}{2}}+(DU_I^2+DV_I^2)^{\frac{1}{2}}D2U_I]. \quad \text{(A11)}$$

There is also an analogous expression for DTY_I.

The required values of U_{IS-1}, V_{IS-1} are obtained from Eqs. (A1) and (A2).

We can now use the calculated value for dU_{IS}/dx to substitute in Eq. (A4) for W_{IS} and then obtain dV_{IS}/dx from the following equation which holds for general values of I by setting $I=IS$. Thus,

$$\frac{dV_I}{dx}=[(1-U_I)/\mathrm{Ro}+e^{-\zeta_I}DTY_I-e^{-\zeta_I}W_IDV_I]/U_I. \quad \text{(A12)}$$

At this stage if we know the U and V profiles for some value of x, we can calculate numerical values of dU_{IS}/dx, W_{IS} and dV_{IS}/dx. We now proceed outward for $I=IS+1$, $IS+2$, $\cdots$, $N-1$, where z_N is the boundary between our logarithmic line spacing region and the linear line spacing region. The relations used for dU_I/dx and W_I based on finite difference representations of Eqs. (12) and (14), are

$$\frac{dU_I}{dx}=\frac{\{V_I/\mathrm{Ro}+e^{-\zeta_I}DTX_I-[e^{-\zeta_I}W_{I-1}-(\Delta\zeta/2)e^{-\Delta\zeta/2}(dU_{I-1}/dx)]dU_I\}}{U_I-e^{-\Delta\zeta/2}(U_{I+1}-U_{I-1})/4}. \quad \text{(A13)}$$

$$W_I=W_{I-1}-\frac{\Delta\zeta}{2}\left(\frac{dU_I}{dx}+\frac{dU_{I-1}}{dx}\right)\exp(\zeta_I-\Delta\zeta/2). \quad \text{(A14)}$$

Eq. (A12) is now used to calculate dV_I/dx.

In this way we can work outward from the wall to the height z_{N-1} above which we alter the spacing of the discretization points from logarithmic to linear. In order to achieve a smooth transition we choose the z' spacing of the outer lines such that $\Delta z=z_N-z_{(N-LBS)}$ where LBS is some small integer. In order to avoid overwriting of arrays in the computer, z_N was identical with z_{50} and z_{N-LBS} with z_{49}, thus placing a restraint on N so that we must have $N\leq 48$. We denote the upper limit of our region as z_{NN} and assume $U_{NN+1}=1$, $V_{NN+1}=0$. We can now use finite difference representations of Eqs. (3), (4) and (5) to find dU_I/dx, W_I and dV_I/dx for $I=50,51,\cdots,NN$ using

$$\frac{dU_I}{dx}=\frac{\{V_I/\mathrm{Ro}+DTX_I-[(W_{I-1}-(\Delta z/2)(dU_{I-1}/dx))]DU_I\}}{U_I-(U_{I+1}-U_{I-1})/4}, \quad \text{(A15)}$$

$$W_I=W_{I-1}-\frac{\Delta z}{2}\left(\frac{dU_I}{dx}+\frac{dU_{I-1}}{dx}\right), \quad \text{(A16)}$$

$$\frac{dV_I}{dx}=\frac{[(1-U_I)/\mathrm{Ro}]+DTY_I-W_IDV_I}{U_I}, \quad \text{(A17)}$$

where DU_I, $D2U_I$ and DTX_I are now given by:

$$DU_I=(U_{I+1}-U_{I-1})/2\Delta z, \quad \text{(A18)}$$

$$D2U_I=(U_{I+1}-2U_I+U_{I-1})/(\Delta z)^2, \quad \text{(A19)}$$

$$DTX_I=2l'(z_I)\left(\frac{dl'}{dz}\right)_{z'=z_I}(DU_I^2+DV_I^2)^{1/2}DU_I+l'^2(z_I)[(DU_I^2+DV_I^2)^{1/2}D2U_I+DU_I(DU_ID2U_I+DV_ID2V_I)\times(DU_I^2+DV_I^2)^{-\frac{1}{2}}], \quad \text{(A20)}$$

and similar expressions for DV_I, $D2V_I$ and DTY_I.

We are thus able to calculate $(\partial U'/\partial x')$ and $(\partial V'/\partial x')$ at our discretization points and so use the Runge-Kutta method to solve the system of ordinary differential equations.

TABLE 1. Parameters used in numerical solution ($m=10$).

	$\Delta\zeta$	IS	z_{IS}	N	LBS
$x'=0\rightarrow 10$	0.266	6	3.9	32	4
$x'=10\rightarrow 10^2$	0.532	4	7.4	16	2
$x'=10^2\rightarrow 10^3$	0.532	6	23.3	16	2
$x'=10^3\rightarrow 10^4$	0.532	8	69.5	16	2
$x'=10^4\rightarrow 10^5$	1.064	5	203.4	8	1
$x'=10^5\rightarrow 10^6$	1.064	6	591.3	8	1
$x'=10^6\rightarrow 10^7$	1.064	7	1715	8	1
$x'=10^7\rightarrow 10^8$	1.064	7	1715	8	1

Overall parameters: $NN=99$, $z_{NN}=1.65\times10^6$, $\Delta z=3258$, $z_{50}=z_N=4973$.

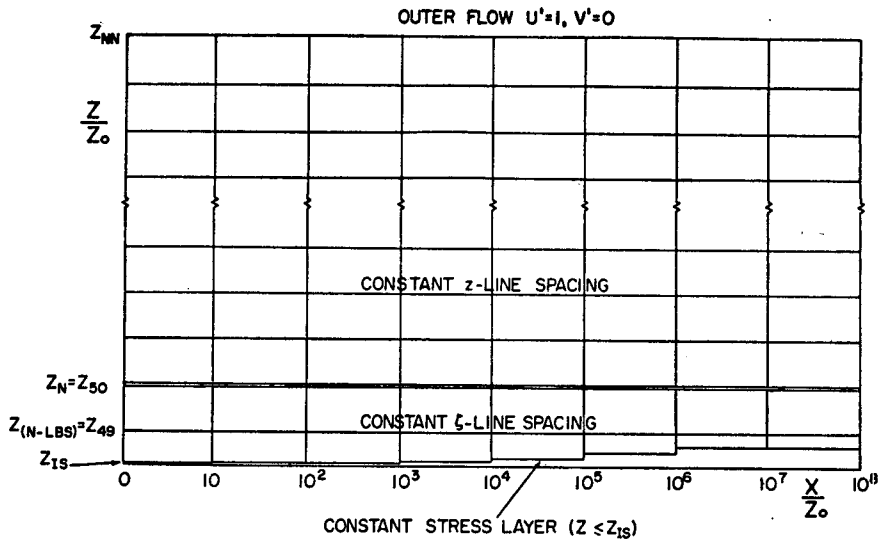

FIG. 8. Region used for numerical solution.

In order to save computer time and still retain accuracy at all downstream distances a procedure of varying IS and also $\Delta\zeta$ in stages as the integration proceeds downstream was adopted. The values of Δz, NN, z_{NN} and z_N are kept constant however throughout, thus placing restraints on the values of $\Delta\zeta$ and LBS that must be used.

Typical values of these and related quantities are given in Table 1.

The values of z_{IS} for $x'=0\rightarrow 10^3$ may seem rather large, but it should be borne in mind that it is a comparatively deep layer that is the primary subject of this investigation. The surface layer is considered in Taylor (1969a) using a similar method and finer line spacings near the ground. Trials using smaller values of z_{IS} indicate that no serious errors are introduced as a result of the use of such a large wall layer. Note that in the case $m=10$ for which the parameters are given, $z_{IS}=3.9$ corresponds to $z/z_0=3.9$, but $z/z_1=0.39$. A sketch of the solution region is given in Fig. 8.

REFERENCES

Elliott, W. P., 1958: The growth of the atmospheric internal boundary layer. *Trans. Amer. Geophys. Union*, **39**, 1048–1054.

Haltiner, G. J., and F. L. Martin, 1957: *Dynamical and Physical Meteorology*. New York, McGraw–Hill, 470 pp.

Lettau, H. H., 1950: A re-examination of the " Leipzig Wind Profile". *Tellus*, **2**, 125–129.

Miyake, M., 1961: Transformation of the atmospheric boundary layer induced by inhomogeneous surfaces. M.Sc. thesis, University of Wasington.

Nickerson, E. C., 1968: Boundary layer adjustment as an initial value problem. *J. Atmos. Sci.*, **25**, 207–213.

Panofsky, H. A., and A. A. Townsend, 1964: Change of terrain roughness and the wind profile. *Quart. J. Roy. Meteor. Soc.*, **90**, 147–155.

Taylor, P. A., 1967: On turbulent wall flows above a change in surface roughness. Ph.D. thesis, University of Bristol.

——, 1969a: On wind and shear stress profiles above a change in surface roughness. *Quart. J. Roy. Meteor. Soc.*, **95** (in press).

——, 1969b: On planetary boundary layer flow under conditions of neutral thermal stability. *J. Atmos. Sci.*, **26**, 427–431.